

Aperiodic CrSc multilayer mirrors for attosecond water window pulses

Alexander Guggenmos,^{1,2,*} Roman Rauhut,¹ Michael Hofstetter,^{1,2}
Samira Hertrich,¹ Bert Nickel,¹ Jürgen Schmidt,¹ Eric M. Gullikson,³ Markus Seibald,⁴
Wolfgang Schnick,⁴ and Ulf Kleineberg^{1,2}

¹Ludwig-Maximilians-Universität München, Fakultät für Physik, Am Coulombwall 1, D-85748 Garching, Germany

²Max-Planck-Institut für Quantenoptik, Hans-Kopfermann-Str. 1, D-85748 Garching, Germany

³Center for X-Ray Optics, Lawrence Berkeley National Lab 2-400, 1 Cyclotron Road, Berkeley, CA 94720, USA

⁴Ludwig-Maximilians-Universität München, Department Chemie, Butenandtstr. 5-13, D-81377 München, Germany
alexander.guggenmos@physik.uni-muenchen.de

Abstract: Extending single attosecond pulse technology from currently sub-200 eV to the so called ‘water window’ spectral range may enable for the first time the unique investigation of ultrafast electronic processes within the core states of bio-molecules as proteins or other organic materials. Aperiodic multilayer mirrors serve as key components to shape these attosecond pulses with a high degree of freedom and enable tailored short pulse pump-probe experiments. Here, we report on chirped CrSc multilayer mirrors, fabricated by ion beam deposition with sub-angstrom precision, designed for attosecond pulse shaping in the ‘water window’ spectral range.

©2013 Optical Society of America

OCIS codes: (320.0320) Ultrafast optics; (320.1590) Chirping; (320.5540) Pulse shaping; (340.7480) X-rays, soft x-rays, extreme ultraviolet (EUV); (310.4165) Multilayer design.

References and links

1. M. Hentschel, R. Kienberger, Ch. Spielmann, G. A. Reider, N. Milosevic, T. Brabec, P. Corkum, U. Heinzmann, M. Drescher, and F. Krausz, “Attosecond metrology,” *Nature* **414**(6863), 509–513 (2001).
2. G. Sansone, F. Kelkensberg, J. F. Pérez-Torres, F. Morales, M. F. Kling, W. Siu, O. Ghafur, P. Johnsson, M. Swoboda, E. Benedetti, F. Ferrari, F. Lépine, J. L. Sanz-Vicario, S. Zherebtsov, I. Znakovskaya, A. L’huillier, M. Yu. Ivanov, M. Nisoli, F. Martín, and M. J. J. Vrakking, “Electron localization following attosecond molecular photoionization,” *Nature* **465**(7299), 763–766 (2010).
3. M. Schultze, M. Fiess, N. Karpowicz, J. Gagnon, M. Korbman, M. Hofstetter, S. Neppl, A. L. Cavalieri, Y. Komninos, Th. Mercouris, C. A. Nicolaides, R. Pazourek, S. Nagele, J. Feist, J. Burgdörfer, A. M. Azeer, R. Ernstorfer, R. Kienberger, U. Kleineberg, E. Goulielmakis, F. Krausz, and V. S. Yakovlev, “Delay in Photoemission,” *Science* **328**(5986), 1658–1662 (2010).
4. S. Neppl, R. Ernstorfer, E. M. Bothschafter, A. L. Cavalieri, D. Menzel, J. V. Barth, F. Krausz, R. Kienberger, and P. Feulner, “Attosecond Time-Resolved Photoemission from Core and Valence States of Magnesium,” *Phys. Rev. Lett.* **109**(8), 087401 (2012).
5. M. Hofstetter, M. Schultze, M. Fieß, B. Dennhardt, A. Guggenmos, J. Gagnon, V. S. Yakovlev, E. Goulielmakis, R. Kienberger, E. M. Gullikson, F. Krausz, and U. Kleineberg, “Attosecond dispersion control by extreme ultraviolet multilayer mirrors,” *Opt. Express* **19**(3), 1767–1776 (2011).
6. M. Suman, G. Monaco, M.-G. Pelizzo, D. L. Windt, and P. Nicolosi, “Realization and characterization of an XUV multilayer coating for attosecond pulses,” *Opt. Express* **17**(10), 7922–7932 (2009).
7. G. Sansone, L. Poletto, and M. Nisoli, “High-energy attosecond light sources,” *Nat. Photonics* **5**(11), 655–663 (2011).
8. E. Goulielmakis, M. Schultze, M. Hofstetter, V. S. Yakovlev, J. Gagnon, M. Uiberacker, A. L. Aquila, E. M. Gullikson, D. T. Attwood, R. Kienberger, F. Krausz, and U. Kleineberg, “Single-cycle nonlinear optics,” *Science* **320**(5883), 1614–1617 (2008).
9. T. Gorniak, R. Heine, A. P. Mancuso, F. Staier, C. Christophis, M. E. Pettitt, A. Sakdinawat, R. Treusch, N. Guerassimova, J. Feldhaus, C. Gutt, G. Grübel, S. Eisebitt, A. Beyer, A. Götzhäuser, E. Weckert, M. Grunze, I. A. Vartanyants, and A. Rosenhahn, “X-ray holographic microscopy with zone plates applied to biological samples in the water window using 3rd harmonic radiation from the free-electron laser FLASH,” *Opt. Express* **19**(12), 11059–11070 (2011).
10. Ch. Spielmann, N. H. Burnett, S. Sartania, R. Koppitsch, M. Schnürer, C. Kan, M. Lenzner, P. Wobrauschek, and F. Krausz, “Generation of Coherent X-rays in the Water Window Using 5-Femtosecond Laser Pulses,” *Science* **278**(5338), 661–664 (1997).

11. N. N. Salashchenko and E. A. Shamov, "Short-period X-ray multilayers based on Cr/Sc," *Opt. Commun.* **134**(1-6), 7–10 (1997).
12. F. Schäfers, "Multilayers for the EUV/soft X-ray range," *Physica B* **283**(1-3), 119–124 (2000).
13. E. M. Gullikson, F. Salmassi, A. L. Aquila, and F. Dollar, "Progress in short period multilayer coatings for water window applications," <http://www.osti.gov/bridge/servlets/purl/932470-IG3P4J/932470.pdf>.
14. Y. Uspenskii, D. Burenkov, T. Hatano, and M. Yamamoto, "Optimal Design of Multilayer Mirrors for Water-Window Microscope Optics," *Opt. Rev.* **14**(1), 64–73 (2007).
15. T. Tsuru, "Reflection Passband Broadening by Aperiodic Designs of EUV/Soft X-ray Multilayers," *AIP Conf. Proc.* **879**, 1524–1530 (2007).
16. F. Bridou, F. Delmotte, Ph. Troussel, and B. Villette, "Design and fabrication of X-ray non-periodic multilayer mirrors: Apodization and shaping of their spectral response," *Nucl. Instrum. Methods* **680**, 69–74 (2012).
17. C. Bourassin-Bouchet, M. Stephens, S. de Rossi, F. Delmotte, and P. Chavel, "Duration of ultrashort pulses in the presence of spatio-temporal coupling," *Opt. Express* **19**(18), 17357–17371 (2011).
18. A. J. Verhoef, A. V. Mitrofanov, X. T. Nguyen, M. Krikunova, S. Fritzsche, N. M. Kabachnik, M. Drescher, and A. Baltuška, "Time-and-energy-resolved measurement of Auger cascades following Kr 3d excitation by attosecond pulses," *New J. Phys.* **13**(11), 113003 (2011).
19. H. Jiang, J. Zhu, J. Xu, X. Wang, Z. Wang, and M. Watanabe, "Determination of layer-thickness variation in periodic multilayer by X-ray reflectivity," *J. Appl. Phys.* **107**(10), 103523 (2010).
20. F. Eriksson, G. A. Johansson, H. M. Hertz, E. M. Gullikson, U. Kreissig, and J. Birch, "14.5% near-normal incidence reflectance of Cr/Sc x-ray multilayer mirrors for the water window," *Opt. Lett.* **28**(24), 2494–2496 (2003).
21. A. V. Tikhonravov, M. K. Trubetskov, and G. W. DeBell, "Optical coating design approaches based on the needle optimization technique," *Appl. Opt.* **46**(5), 704–710 (2007).
22. H. G. Tompkins and E. A. Irene, in *Handbook of ellipsometry*, William Andrew, ed. (Springer Verlag GmbH, 2005).
23. F. A. Jenkins and H. E. White, in *Fundamentals of Optics*, 4th ed. (McGraw-Hill, Inc. 1981).
24. S. A. Yulin, F. Schaefer, T. Feigl, and N. Kaiser, "High-performance Cr/Sc multilayers for the soft X-ray range," *Proc. SPIE* **5193**, 172–176 (2004).
25. E. M. Gullikson, S. Mrowka, and B. B. Kaufmann, "Recent developments in EUV reflectometry at the Advanced Light Source," *Proc. SPIE* **4343**, 363–373 (2001).
26. L. Nénot and P. Croce, "Caractérisation des surfaces par réflexion rasante de rayons X. Application à l'étude du polissage de quelques verres silicates," *Rev. Phys. Appl. (Paris)* **15**(3), 761–779 (1980).
27. B. L. Henke, E. M. Gullikson, and J. C. Davis, "X-ray interactions: photoabsorption, scattering, transmission, and reflection at E=50-30000 eV, Z=1-92," *At. Data Nucl. Data Tables* **54**(2), 181–342 (1993).
28. E. Spiller, in *Soft X-ray optics*, (SPIE Optical Engineering Press, Bellingham, USA, 1994).
29. D. H. Ko, K. T. Kim, J. Park, J.-Lee, and C. H. Nam, "Attosecond chirp compensation over broadband high-order harmonics to generate near transform-limited 63 as pulses," *New J. Phys.* **12**(6), 063008 (2010).
30. A. L. Cavalieri, E. Goulielmakis, B. Horvath, W. Helml, M. Schultze, M. Fieß, V. Pervak, L. Veisz, V. S. Yakovlev, M. Uiberacker, A. Apolonski, F. Krausz, and R. Kienberger, "Intense 1.5-cycle near infrared laser waveforms and their use for the generation of ultra-broadband soft-x-ray harmonic continua," *New J. Phys.* **9**(7), 242 (2007).
31. P. Heissler, R. Hörlein, J. M. Mikhailova, L. Waldecker, P. Tzallas, A. Buck, K. Schmid, C. M. S. Sears, F. Krausz, L. Veisz, M. Zepf, and G. D. Tsakiris, "Few-Cycle Driven Relativistically Oscillating Plasma Mirrors: A Source of Intense Isolated Attosecond Pulses," *Phys. Rev. Lett.* **108**(23), 235003 (2012).
32. A. Borot, A. Malvache, X. Chen, A. Jullien, J.-P. Geindre, P. Audebert, G. Mourou, F. Quéré, and R. Lopez-Martens, "Attosecond control of collective electron motion in plasmas," *Nat. Phys.* **8**(5), 416–421 (2012).
33. J. A. Wheeler, A. Borot, S. Monchocé, H. Vincenti, A. Ricci, A. Malvache, R. Lopez-Martens, and F. Quéré, "Attosecond lighthouses from plasma mirrors," *Nat. Photonics* **6**(12), 829–833 (2012).
34. E. Gustafsson, T. Ruchon, M. Swoboda, T. Remetter, E. Pourtal, R. López-Martens, Ph. Balcou, and A. L'Huillier, "Broadband attosecond pulse shaping," *Opt. Lett.* **32**(11), 1353–1355 (2007).
35. R. Hörlein, Y. Nomura, P. Tzallas, S. G. Rykovanov, B. Dromey, J. Osterhoff, Zs. Major, S. Karsch, L. Veisz, M. Zepf, D. Charalambidis, F. Krausz, and G. D. Tsakiris, "Temporal characterization of attosecond pulses emitted from solid-density plasmas," *New J. Phys.* **12**(4), 043020 (2010).
36. A.-S. Morlens, P. Balcou, P. Zeitoun, C. Valentin, V. Laude, and S. Kazamias, "Compression of attosecond harmonic pulses by extreme-ultraviolet chirped mirrors," *Opt. Lett.* **30**(12), 1554–1556 (2005).
37. G. Sansone, E. Benedetti, F. Calegari, C. Vozzi, L. Avaldi, R. Flammini, L. Poletto, P. Villoresi, C. Altucci, R. Velotta, S. Stagira, S. De Silvestri, and M. Nisoli, "Isolated Single-Cycle Attosecond Pulses," *Science* **314**(5798), 443–446 (2006).
38. V. Yakovlev and G. Tempea, "Optimization of Chirped Mirrors," *Appl. Opt.* **41**(30), 6514–6520 (2002).
39. A. Aquila, F. Salmassi, and E. Gullikson, "Metrologies for the phase characterization of attosecond extreme ultraviolet optics," *Opt. Lett.* **33**(5), 455–457 (2008).
40. C. Bourassin-Bouchet, S. de Rossi, J. Wang, E. Meltchakov, A. Giglia, N. Mahne, S. Nannarone, and F. Delmotte, "Shaping of single-cycle sub-50-attosecond pulses with multilayer mirrors," *New J. Phys.* **14**(2), 023040 (2012).
41. H. G. Muller, "Reconstruction of attosecond harmonic beating by interference of two-photon transitions," *Appl. Phys. B* **74**(9), s17–s21 (2002).

42. R. López-Martens, K. Varjú, P. Johnsson, J. Mauritsson, Y. Mairesse, P. Salières, M. B. Gaarde, K. J. Schafer, A. Persson, S. Svanberg, C.-G. Wahlström, and A. L’huillier, “Amplitude and Phase Control of Attosecond Light Pulses,” *Phys. Rev. Lett.* **94**(3), 033001 (2005).
 43. Y. Mairesse, A. de Bohan, L. J. Frasinski, H. Merdji, L. C. Dinu, P. Monchicourt, P. Breger, M. Kovačev, R. Taïeb, B. Carré, H. G. Muller, P. Agostini, and P. Salières, “Attosecond Synchronization of High-Harmonic Soft X-rays,” *Science* **302**(5650), 1540–1543 (2003).
-

1. Introduction

Multilayer XUV/soft X-ray mirrors are key components for steering attosecond pulses from high harmonic radiation [1]. These pulses pave the way towards the observation of electron dynamics in atoms, molecules or solid surfaces/nanostructures with an unprecedented temporal precision [2–4]. Aperiodic multilayer mirrors exhibit the required degree of freedom for the tailored shaping of attosecond pulses in the XUV/soft X-ray range [5,6]. Extending the current attosecond technology [7] to the so called ‘water window’ spectral range between the carbon 1s (284 eV) and oxygen 1s (543 eV) states may enable not only the generation of ever shorter isolated pulses [8], but could allow to access deeper electron core levels which may facilitate the investigation of electron dynamics in bio-molecules [9,10]. The material combination of chromium (Cr) and scandium (Sc) is the most appropriate choice for multilayer mirrors in the 250-400 eV photon energy range [11,12], where a maximum normal incidence reflectivity up to 32.1% (in the vicinity of the Sc 2p-edge at 398.7 eV) and a typical interface roughness down to 0.32 nm has been realized for periodic small-bandwidth multilayer by magnetron sputtering technique [13]. Up to now broadband aperiodic CrSc multilayer mirrors have been investigated only theoretically for the ‘water window’ [14,15] or have been realized at grazing angles for the keV range [16]. Previous experiments have shown that aperiodic multilayer mirrors can control the attosecond pulse dispersion around 100 eV [5,6,17] being used for resonant excitation of distinct atomic core states [18]. Extending this control, into the ‘water window’ spectral range, requires multilayer optics of sub-angstrom layer precision as their spectral amplitude and phase are extremely sensitive to even the smallest thickness errors of only a fraction of the nominal layer thickness [19] being typically around 1 nm [20]. Here we present one periodic and two aperiodic chirped CrSc multilayer mirrors, designed via numerical algorithms [21], fabricated by ion beam deposition, and characterized by hard- and soft X-ray reflectometry. We show excellent agreement between the simulated reflectivity (based on the ideal multilayer design) and the measured reflectivity, which allows for a retrieval of the experimentally realized multilayer stack structure. By using the measured reflectivity and calculated spectral phase data (derived from the experimental multilayer structure) the temporal response to a chirped single attosecond pulse at ~320 eV has been calculated.

2. Ion beam deposition methodology

2.1 Deposition procedure of the multilayer

Periodic small bandwidth CrSc multilayer mirrors, as well as aperiodic broadband multilayer mirrors, have been fabricated using a load-locked dual ion beam deposition machine, utilizing (neutralized) 600 eV krypton ions at a background pressure of 10^{-7} Pa, sketched in Fig. 1.

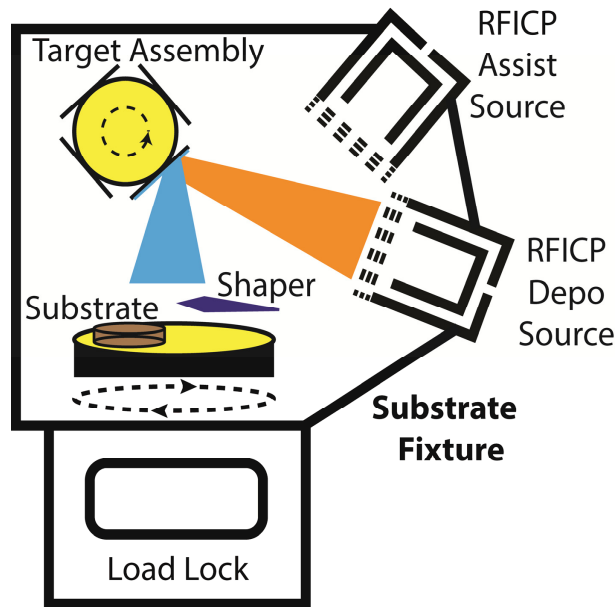


Fig. 1. Schematic setup of the dual ion beam deposition system with load locked sample transfer, four target assemblies, beam shaper and rotating substrate holder.

Each layer thickness has been controlled via its deposition time. Typical sputter rates for both materials are below 0.1 nm per second and have been calibrated using surface profilometry as well as in situ spectral ellipsometry. Sputter time calculations are based on a numerical model, to compensate both for inter-diffusion losses and systematic deposition variations, e.g. shutter response times. The deposition system contains an automatic sample load lock for substrates up to 6 inch, two filament-less radio frequency ion beam sources for target material sputtering (deposition source), as well as ion-assisted deposition (assist source) and four target wheels (400 mm). The substrate holder is spinning during deposition with a spinning frequency of 40 rpm and a R/ θ shaper is being used for shaping the particle flux laterally for graded multilayer growth or high lateral homogeneity film thickness growth.

2.2 Lateral homogeneity and vertical precision

A shaper has been designed to improve the lateral homogeneity as displayed in Fig. 2(a). Deposition rates with and without the shaper have been determined by surface profilometry and XUV reflectivity measurements (comparing the central energy) on a set of molybdenum and silicon (MoSi) multilayer mirrors at various radial positions on the substrate holder. The lateral homogeneity could be improved from about $\pm 5\%$ to less than $\pm 0.5\%$ across the full diameter of the substrate holder. For typical 1 inch substrates the maximum homogeneity deviation is less than 0.2%. The shaper is routinely used for the CrSc multilayer deposition results described in the following.

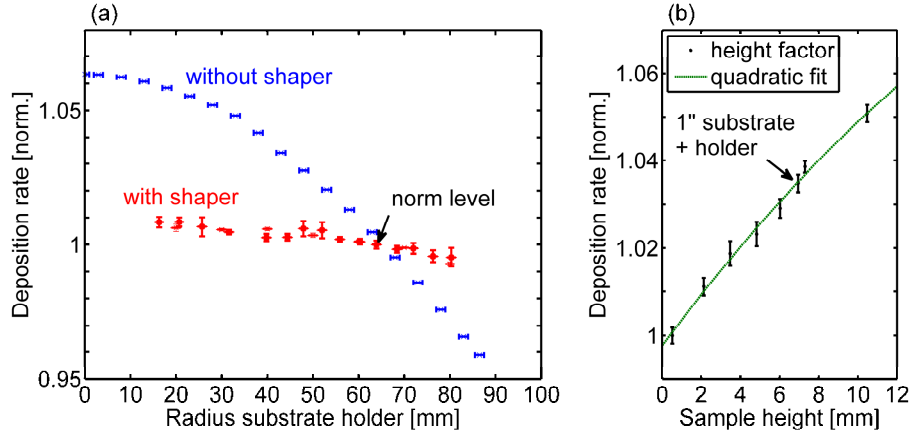


Fig. 2. (a) Lateral (radial) homogeneity of the deposition rates with (red) and without shaper (blue). (b) Rate dependence on the sample height. A quadratic fit coincides quite well with the measured data, since the tapered surface is quadratic dependent on the distance.

Besides lateral homogeneity, the deposition rate depends as well on the sample height and has to be understood and taken into account for a correct mirror design implementation. This pure geometrical dependence can be retrieved analytically from the distance D between the imaginary target point of divergence and the substrate holder as the tapered surface of the ablated material beam scales quadratic with the distance. The relation of the sputter rate dependent on the sample height reads like:

$$\Gamma = \frac{N}{A \cdot 1s} \Leftrightarrow \frac{\Gamma_2}{\Gamma_1} = \frac{A_1}{A_2} = \left(\frac{d_1}{d_2} \right)^2 = \left(\frac{D-h_1}{D-h_2} \right)^2, \quad (1)$$

where Γ indicates the rate, N the number of particles, A the area, h the sample height and d is the distance from the sample surface to the extended target focus as imaginary point source (1: reference norm level, 2: various sample heights). The target rates have been calibrated by a lift-off procedure and consecutive surface profilometry. Figure 2(b) shows the measured deposition rate normalized to a 525 μm thick standard silicon wafer. The deposition rate of a standard 1 inch substrate deviates from this silicon wafer by $\sim 3.5\%$ and would manifest itself in an equal shift in the central energy.

3. Multilayer deposition precision

3.1 Study of the top layer oxidation

Detailed analysis of the top layer of a multilayer mirror is essential to correctly model its reflectivity as it influences the superposition of the incident and reflected radiation. Many materials oxidize when being brought to atmosphere, where sputtered material is lost to build the 'natural' oxide layer. We use spectral ellipsometry in situ and ex-situ within a wavelength range of 380-1800 nm to study such oxidation processes [22]. Spectral ellipsometry allows one to retrieve both the optical constants and the layer thicknesses of simple structures from the measured ellipsometry parameters

$$\tan \psi = \left| r_p / r_s \right| \quad \text{and} \quad \Delta = \varphi_p - \varphi_s, \quad (2)$$

where $r_{p,s}$ are the reflection coefficients and $\varphi_{p,s}$ indicates the phase of the p and s polarization, as a function of the spectral wavelength. An about 8 nm thick single layer of the material (Cr, Sc) was deposited on silicon wafers. The natural SiO_2 -layer thickness of the wafer was retrieved by ellipsometry before the coating and the grown material thickness was

analyzed directly after the coating process without bringing samples to air. We fitted the measured data with a three layer (Si, SiO₂, Cr/Sc) model, displayed in Fig. 3.

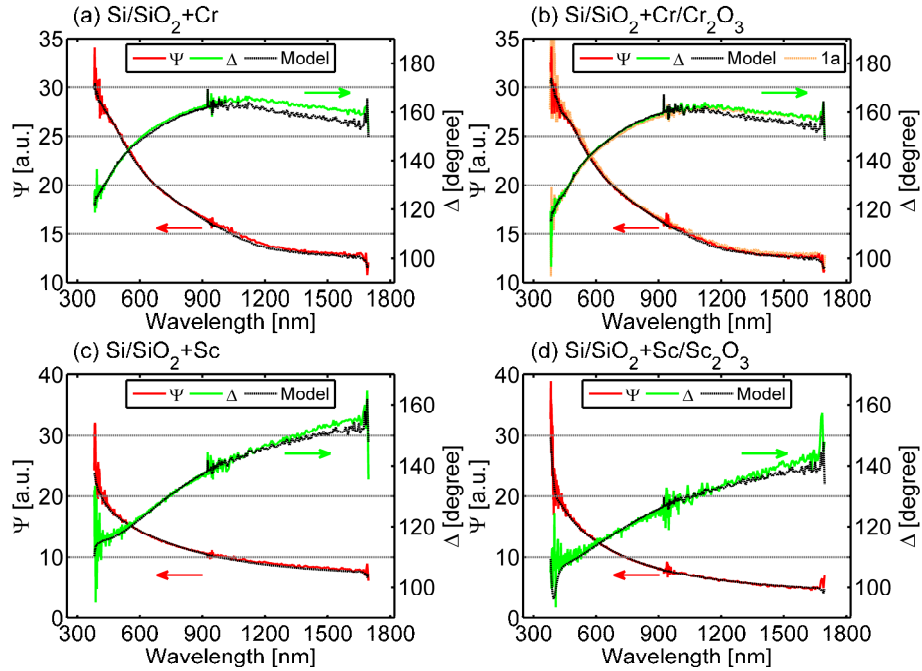


Fig. 3. Ellipsometry parameters psi (red) and delta (green) and the corresponding fitted model (dashed black). Data is taken from samples with pure 8 nm thick layers of (a) chromium and of (c) scandium, and is compared to data measured after 24h oxidation (b) Cr/Cr₂O₃, and of (d) Sc/Sc₂O₃, respectively. In (b) additional data after one year of oxidation is included, showing no measurable change and indicating that chromium is well suited as passivation layer.

After analysis, the samples have been brought to air for 24 hours, before being analyzed again to study the built up oxide layers and the thickness loss of the material layer from which it is built. The optical constants of chromium and scandium have been measured previously from optically thick bulk samples. The optical constants for chromium oxide were taken from the *Woolam* database whereas scandium oxide was approximated with a Cauchy-layer [23] (with the Cauchy parameters $A = 1.163$, $B = 0.01493$, $C = 0.0065$) since it is impossible to measure the optical constants of such thin dielectric layers directly. As result, we found that a loss of 0.31 ± 0.04 nm of chromium forms a 1.40 ± 0.46 nm thick Cr₂O₃ layer and 2.92 ± 0.29 nm pure scandium forms a 6.72 ± 0.24 nm thick Sc₂O₃ layer. This is in full agreement with profilometry which showed a gain of 1.3 ± 0.7 nm for Cr/Cr₂O₃ and 3.9 ± 0.8 nm for Sc/Sc₂O₃ compared to a pure 200 nm bulk. Throughout the following chapters reflectivity simulations and designs take into account the built up oxide.

3.2 Mirror design implementation

Beside systematic deviations of the sputter machine and analyses of the top layer oxidation, last but not least, detailed knowledge about the interface losses of each distinct material combination is important to ensure a correct simulation and implementation of a multilayer. The interface loss of our CrSc multilayer system has been analyzed in comparative studies of single layer and multilayer stacks using again surface profilometry. Our measurements showed no interface loss for our ion beam sputtered CrSc multilayer system in contrast to magnetron sputtered systems [13].

3.3 Characterization by soft/hard X-ray reflectometry

We have evaluated the vertical periodicity accuracy [24] with respect to systematic and random layer thickness deviations inside the CrSc multilayer system, by fabricating a periodic CrSc multilayer mirror with an intended period thickness of $d = 1.953$ nm and a period number of $N = 400$ on a Si (100) substrate. The mirror design was chosen according to a near normal incidence (5 degree off normal) peak reflectivity at a photon energy of 320 eV. The total deposition time of this multilayer system was about 5 h. The periodic CrSc multilayer has been analyzed by soft X-ray reflectometry at the reflectometry beamline 6.3.2 at the Advanced Light Source [25]. The results are depicted in Fig. 4(a). Figure 4(b) shows additionally the witness sample, measured now by Mo- K_{α} grazing incidence reflectometry using a laboratory X-ray diffractometer. Both measurements have been evaluated with respect to the period thickness d , the γ -factor, representing the ratio of the scandium layer thickness to the multilayer period, and the Nevot-Croce [26] interface roughness factor σ . Reflectivity simulations and reflectivity fits have been performed using a self-written multilayer Fresnel code. Throughout this paper, the tabulated values of the atomic scattering factors from Henke and Gullikson [27] for Cr and Sc have been used and bulk layer densities have been assumed.

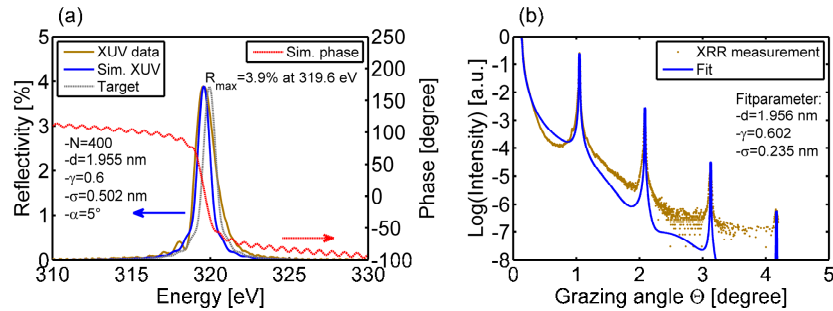


Fig. 4. Characterization of a periodic CrSc multilayer stack, containing 400 periods, by (a) soft X-ray reflectometry and (b) hard X-ray Mo- K_{α} reflectometry. Simulation results are shown for comparison (blue solid lines).

Soft X-ray reflectometry measurement performed at 5 degree off normal reveals a peak photon energy of 319.6 eV and a peak reflectivity of 3.9%. The average period thickness is 1.955 nm and the interface roughness can be estimated to 0.502 nm. The measured reflectivity bandwidth is only slightly larger than expected from the simulation. This indicates a very high vertical periodicity of the deposited multilayer stack with almost negligible random thickness errors. This is confirmed by hard X-ray grazing incidence reflectometry. It reveals a period thickness of 1.956 nm with a multilayer interface roughness of only 0.235 nm, again with very sharp and high contrast Bragg peaks due to the high periodicity of the multilayer stack. While the period thickness and the γ -ratio of both measurements almost perfectly agree, the deviation in the evaluated interface roughness parameter (0.502 nm to 0.235 nm) can be attributed to contamination of the Sc layers. An energy dispersive X-ray spectroscopy measurement indicates $\sim 13\%$ Cu contamination stemming from the target backing plate, which severely affects the soft X-ray peak reflectivity, while it has only minor influence to the hard X-ray reflectometry measurement. For the aperiodic multilayer results described in chapter 4, we have suppressed the contamination of the Sc layers by mounting a larger Sc sputtering target, which diminishes the spill-out of the ion beam on the backing plate. Furthermore, the different penetration depth of the soft and hard X-ray radiation may reveal different roughness values, because accumulating roughness as well as the interface Power Spectral Density [28] is weighted differently.

3.4 Characterization by surface profilometry

As third measurement, the total multilayer stack thickness has been measured by surface profilometry. A set of 24 line scans across different positions of a shadowed deposition edge has been performed. The measured overall thickness together with the mean value and the targeted total stack thickness, based on the calibrated single layer deposition rates of Cr and Sc, is plotted in Fig. 5. The average total stack thickness of 782.959 nm, with a standard deviation of $SD = 0.703$ nm, differs from the target value (782.3 nm) only by about 0.6 nm (after the deposition of 400 periods).

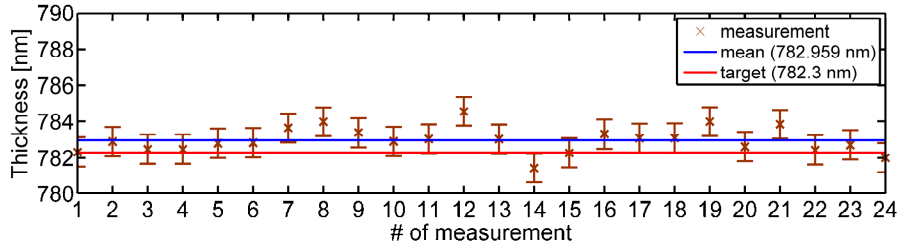


Fig. 5. Total CrSc multilayer stack thickness (same multilayer as in Fig. 4) evaluated from 24 thickness measurements by surface profilometry. Also shown are the mean value and the target stack thickness from calibrated deposition rates.

3.5 Comparison of the methods

In summary the retrieved data from different measurement techniques shows a remarkable agreement with the design based on the model in section 3.2, listed in Table 1. The absolute period (layer) deviation is 0.15%. This is the necessary prerequisite for the fabrication of aperiodic chirped multilayer coatings as will be proven in the following. Both the spectral reflectivity amplitude and the phase respond very sensitively to even the smallest layer thickness deviations on an atomic 0.1 nm scale.

Table 1. Comparison of the evaluated total stack thickness, multilayer period d , interface roughness σ , thickness ratio γ and the period deviation from the target.

Method	Total [nm]	d [nm]	σ [nm]	γ	Deviation[%]
Target	782.3	1.953		0.6	
Profilometry	782.959	1.9546			0.08
XRR	783.5	1.956	0.235	0.602	0.15
XUV	783.1	1.955	0.502	0.6	0.10

4. Chirped multilayers

Based on the layer accuracy achieved on the periodic CrSc multilayer results, as presented in chapter 3, we have simulated and optimized a set of two different aperiodic broadband CrSc multilayer mirrors aiming for the reflection of single attosecond pulses from the high harmonic plateau in the ‘water window’ spectral range around a photon energy of 326 eV. High Harmonic Generation (HHG) sources producing single isolated attosecond pulses, with pulse durations of 80 as [8] or trains of 63 as pulses [29], are possible based on few cycle intense near-infrared (NIR) laser pulses from carrier envelope phase stabilized Ti:sapphire amplifiers, which are converted into a high harmonic spectrum ranging into the XUV spectral range by non-linear frequency conversion in a rare gas medium (e.g. Ar, Ne, He) [3,30] or solid [31–33]. In the past XUV optics have been used to filter and shape these single attosecond pulses from the almost unmodulated plateau region of the high harmonic spectrum [34,35] and compress these pulses down to its Fourier limit by dispersion correction [36]. While time resolved attosecond experiments have been achieved in the sub 100 eV XUV photon energy range [3,37], very recently, with improved laser sources and multilayer optics,

this time resolution has been extended to the 100-150 eV photon energy range [4]. With ever improving few cycle laser development towards higher pulse energies, this regime will soon be extended into the ‘water window’ soft X-ray spectral range, making new exciting time resolved attosecond experiments on e.g. charge transfer dynamics in bio-molecules possible. Using thin filters for attosecond pulse shaping in this energy regime is limited to fixed opening and absorption edges of the used material and thus restricts the degree of freedom. This leaves multilayer mirrors as the only components for tailor-made spectral filtering and shaping an attosecond ‘water window’ pulse. For that reason, we have developed a chirped aperiodic CrSc multilayer optimized for reflecting sub-70 as pulses from HHG at central photon energy of 326.3 eV (Ar L₁-edge) with a bandwidth of about 30 eV for future resonant attosecond photo ionization experiments.

4.1 Characteristics of the chirped CrSc multilayer mirrors

The two different aperiodic CrSc multilayer mirrors have been optimized by the thin film program Optilayer, a Fresnel code coupled to a needle optimization algorithm [21,38]. While one multilayer has been designed for introducing an averaged negative chirp (within this paper, the group delay dispersion is the negative second derivative of the spectral phase, $GDD = -d^2\phi/d\omega^2$) of approximately -8000 as^2 to compress a possible positive chirp of the high harmonic plateau, a second mirror with similar parameters has been designed to introduce an averaged positive chirp of approximately $+8000 \text{ as}^2$. Both mirrors have been designed such that their central energy coincides with the L₁-edge of Argon (326.3 eV) at an angle of incidence of 45 degree. The optimized stack design for the negatively (a) and positively (b) chirped CrSc multilayer is shown in Fig. 6, each of them containing around 95 individual layers. The design has been chosen according to their robustness of GDD against small layer thickness errors, which will be proven at the end of this section. Typical layer thicknesses are between 1 and 2 nm, with thinnest layers going down to 0.5 nm. For both designs a top layer of 1.4 nm Cr₂O₃ out of 0.3 nm Cr has been included in the model. These designs principally prove the large degree of freedom in customizing ‘water window’ attosecond pulses both in space and time using CrSc multilayer mirrors.

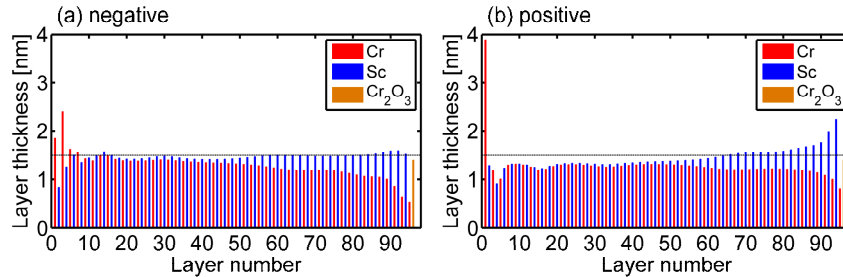


Fig. 6. Multilayer stack designs of the aperiodic CrSc multilayers for the (a) negative and (b) positive chirp. For comparison reasons an arbitrary line with a layer thickness of $d = 1.5 \text{ nm}$ is depicted (dashed).

After the experimental realization of both designs, we first checked the accuracy by surface profilometry. The total stack height, including the oxide layer, for the negative one was calculated to be 131.2 nm and for the positive one 130.9 nm. Out of the profilometry data we retrieved a measured total stack height of $(131.4 \pm 0.6) \text{ nm}$ for the negative and $(131.1 \pm 0.7) \text{ nm}$ for the positive mirror which is in well agreement with the target stack height. The second accuracy check was done by Mo-K_α grazing incidence reflectometry, since this method is well known to be sensitive especially to aperiodic multilayer systems. The measured and fitted data is plotted in Fig. 7.

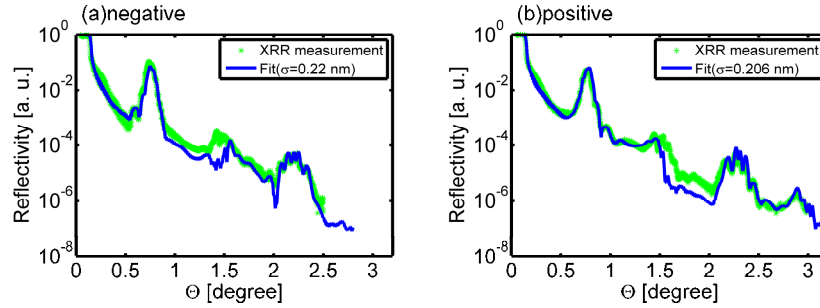


Fig. 7. XRR measurement (green) and the fit (blue) for the negative multilayer mirror in (a) and for the positive one in (b), respectively. The negative mirror has been fitted with a roughness parameter of $\sigma = 0.22$ nm whereas the positive shows a slightly lower value of $\sigma = 0.206$ nm. The noise level of the XRR measurement is on the order of approximately 3.5×10^{-7} . Therefore the measurement data for the negative mirror is clipped at around $\Theta \approx 2.5^\circ$ whereas the positive mirror extends up to $\Theta \approx 3^\circ$.

For the fitting procedure, we assumed a perfect implementation of the start design of Fig. 6, thus no thickness errors were included in the fit. The only fitting parameters we have optimized for the agreement with the measurement data were the roughness parameter and the chromium oxide layer thickness (together with the necessary chromium loss) within the error range which has been determined ellipsometrically in section 3.1. Although there are only these fitting parameters allowed, we find a nearly perfect agreement between the simulated aperiodic systems and the XRR measurement. Together with the profilometry data, this is a strong indication of an accurate implementation of the chirped multilayer systems. XUV reflectometry measurements of both chirped multilayer systems are presented and discussed in chapter 4.2.

The introduction of chirp upon reflection can be visualized by standing wave simulations. The electrical field intensity (electrical field squared), normalized to the incoming intensity, has been calculated from the design at the surface and inside both multilayers and is displayed in Fig. 8. It is clearly shown, that the standing wave peak position decreases in photon energy in case of the negatively chirped system shown in Fig. 8(a), while it increases with increasing depth for the positively chirped multilayer in Fig. 8(b). The negatively chirped mirror thus delays the lower energy pulse spectrum with respect to the higher energy pulse spectrum. The second mirror shows the opposite dispersion effect and was designed for comparison.

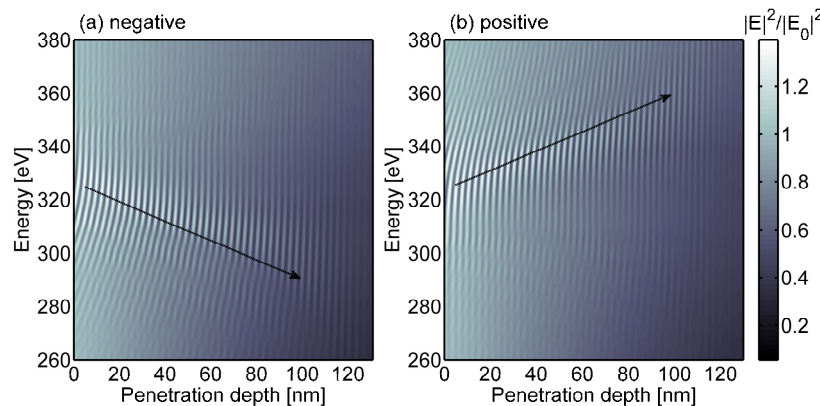


Fig. 8. Calculated field intensity distribution (normalized to incoming intensity) of the standing wave field inside the (a) negatively and (b) positively chirped aperiodic CrSc multilayer. Both multilayer systems have been optimized for an averaged Group Delay Dispersion of approximately ± 8000 as^2 .

4.2 Soft X-ray reflectometry and layer errors

A comparison of the simulated and measured soft X-ray reflectivity for the negatively and positively chirped multilayer mirror is shown in Fig. 9. The measurements were performed by soft X-ray reflectometry at the beamline 6.3.2 of the Advanced Light Source at an incidence angle of 45 degree [25]. The design simulations were performed using a self-written algorithm and the start designs from Optilayer [21]. An average Nevot-Croce roughness factor of $\sigma = 0.49$ nm has been retrieved from simulations to account for interfacial imperfections.

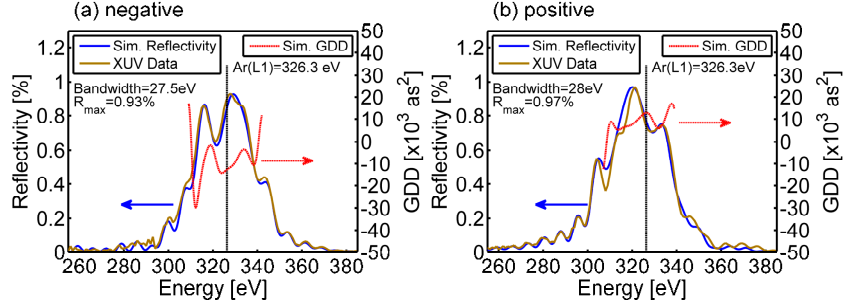


Fig. 9. Soft X-ray reflectivity measurement (brown) and simulation (blue) for the (a) negatively and (b) positively chirped CrSc multilayer together with the corresponding simulated GDD (dashed red).

Both the central energy and the side peaks of the measurements and the designs coincide very well and indicate a nearly perfect experimental implementation of the simulated multilayer stack designs of Fig. 6. Also shown is the calculated evolution of the GDD within the reflectivity bandwidth of both multilayer, indicating an averaged GDD of ± 8000 as^2 . Both multilayers are very similar in terms of peak energy, spectral bandwidth and peak reflectivity and only differ by the sign of their group delay dispersion. Note that the spectral multilayer phase (and thus the GDD) is not accessible by simple reflectivity measurements. Measurements of the spectral phase in soft X-ray reflectometry have been reported by detecting the standing-wave assisted total electron yield from the multilayer surface as a function of the photon energy around the Bragg peak [39,40]. While this method is very suitable for periodic multilayer systems, its accuracy is limited when applied to aperiodic systems with a weak standing wave. On the other hand one can characterize the spectral phase with two attosecond methods, the RABBITT-technique (Reconstruction of Attosecond harmonic Beating By Interference of Two-photon Transitions) [41,42] or by attosecond photoelectron streaking spectroscopy providing access to a full characterization of the reflected attosecond pulse in amplitude and phase [5,8]. However, for the ‘water window’ spectral range the implementation of both attosecond techniques has not been established yet due to a lack of sufficient photon flux from HHG attosecond sources in this spectral range. Here we analyze and estimate the influence of the layer errors on the reflectivity and the GDD via simulations. The rather perfect match of the designed and the measured reflectivity curves in Fig. 9 proves the correct elimination of systematic deposition errors and leaves only random errors to be analyzed. Here we compare both the simulated reflectivity and the GDD of the original design of the negatively chirped multilayer with that of slightly modified designs. The designs have been chosen randomly by juggling each layer thickness within predefined limits and we have calculated the merit function (MF) of the reflectivity as well as the corresponding averaged GDD value to analyze the quality of reflectivity and GDD simulations:

$$MF = \sqrt{\frac{1}{N} \sum_{i=1}^N (R_{Sim,i} - R_{XUV,i})^2}, \quad (3)$$

where N is the total number of wavelength sampling with an integer i representing the position of the sampling equally spaced. 100 designs have been averaged per allowed error and both the reflectivity and the GDD deviations have been calculated. Designs with an overall stack height deviation of more than 0.8% have been left out due to inconsistency with profilometry investigations. From Fig. 10(a) can be deduced, that the average random thickness error is less than 0.5%, corresponding to an average layer thickness error of approximately 0.05 angstrom. Figure 10(b) shows, that the mean GDD value stays nearly constant independently of the layer errors. The upper limit of the layer errors of 0.5% corresponds to a maximum mean GDD error of approximately $\pm 150 \text{ as}^2$. To summarize the results, we have a standard deviation of $\sim 0.024\%$ in the XUV reflectivity and a mean GDD of $-8090 \pm 150 \text{ as}^2$ for our aperiodic negatively chirped CrSc multilayer mirror.

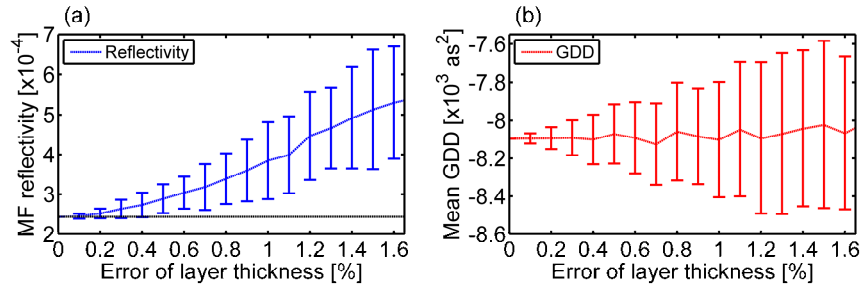


Fig. 10. (a) Merit function for the simulated reflectivity and the XUV measurement for different layer thickness errors. (b) Mean GDD for different layer errors.

4.3 Time domain simulation

An attosecond pulse from the high harmonic plateau regime, with a positive GDD of $+8000 \text{ as}^2$ in the energy range of the mirror, has been assumed, which is reflected off the negatively chirped mirror. The resulting pulse after reflection is displayed both in the spectral and in the temporal domain in Fig. 11. As a result, the pulse is compressed to a single 69 as pulse with an almost symmetric temporal pulse form and very minor pre and post pulse contributions. The pulse is almost compressed to a Gaussian Fourier limit of 66 as given by the spectral bandwidth of the multilayer of 27.5 eV. Please note, that the assumed positive GDD of 8000 as^2 of the HHG plateau at 326 eV probably exaggerates the real GDD in the harmonic spectrum in this photon energy range by a factor of four [43]. However, the development, optimization and fabrication of negatively chirped multilayer mirrors with less GDD in the -1000 as^2 to -2000 as^2 range is even easier to achieve. In this respect, the current results display the high dispersion scenario possible to achieve with a single multilayer reflection.

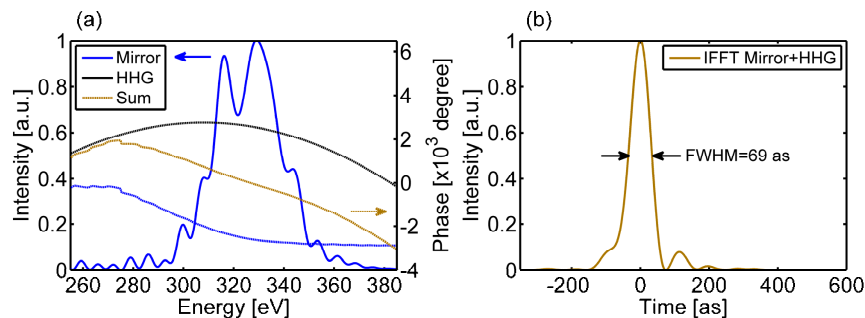


Fig. 11. (a) Intensity of the mirror (blue line) together with the phase for the mirror (dashed blue), HHG (dashed black) and the sum (dashed brown). (b) Simulated temporal pulse response of a positively chirped attosecond pulse from the high harmonic plateau after compression by the negatively chirped CrSc multilayer mirror.

5. Conclusion

We have shown the ability to realize multilayer structures by ion beam deposition with sub-angstrom precision, by compensating all systematic errors which arise from the deposition procedure. Based on that, we have realized two chirped CrSc multilayer mirrors for the ‘water window’ photon energy range with an averaged group delay dispersion of approximately $\pm 8000 \text{ as}^2$. Such chirped mirrors can be used in the near future to e.g. compress single attosecond pulses from the HHG cutoff region to its Fourier limit below 70 as pulse duration. A good agreement between the targeted and measured reflectivity was found and the desired spectral phase was derived from simulations. Direct temporal attosecond pulse measurements by attosecond electron streaking will be a task for the near future, when HHG sources with sufficient photon flux in the cut-off region, applicable to generate single attosecond pulses, reach up to approximately 350 eV.

Acknowledgments

We thankfully acknowledge scientific support and valuable discussions by F. Krausz (MPQ, LMU). This work was supported by the DFG Excellence Cluster “Munich-Centre for Advanced Photonics” (MAP).